

Document downloaded from:

<http://hdl.handle.net/10251/83511>

This paper must be cited as:

Carceller Candau, C.; Soto Pacheco, P.; Boria Esbert, VE.; Guglielmi, M. (2016). Design of Hybrid Folded Rectangular Waveguide Filters With Transmission Zeros Below the Passband. *IEEE Transactions on Microwave Theory and Techniques*. 64(2):475-485. doi:10.1109/TMTT.2015.2510644.



The final publication is available at

<http://dx.doi.org/10.1109/TMTT.2015.2510644>

Copyright Institute of Electrical and Electronics Engineers (IEEE)

Additional Information

(c) 2016 IEEE. Personal use of this material is permitted. Permission from IEEE must be obtained for all other users, including reprinting/ republishing this material for advertising or promotional purposes, creating new collective works for resale or redistribution to servers or lists, or reuse of any copyrighted components of this work in other works.

Design of Hybrid Folded Rectangular Waveguide Filters with Transmission Zeros Below the Passband

Carlos Carceller, *Member, IEEE*, Pablo Soto, *Member, IEEE*, Vicente Boria, *Senior Member, IEEE*,
Marco Guglielmi, *Fellow, IEEE*

Abstract—The design and physical implementation of hybrid folded rectangular waveguide (HFRW) filters providing multiple transmission zeros (TZs) below the passband are considered in this paper. These structures offer great flexibility to locate the TZs in a wide frequency range. Different implementations have been considered, each one offering certain advantages in terms of ease of manufacture, number of TZs and their separation from the passband. A simple design procedure for these structures is also described. Measurements of a manufactured 5-pole filter prototype, and simulations (obtained with several available commercial software tools) for different triplet sections, fully validate the novel configurations proposed in this work.

Index Terms—Waveguide filters, quasi-elliptic filters, tuning-less filters.

I. INTRODUCTION

NOWADAYS, a wide variety of communication systems must coexist within the limited electromagnetic spectrum allocated for many commercial applications at microwave frequencies. In this crowded environment, the interference of a system into neighboring frequency bands becomes a critical issue, especially as capacity requirements are increasingly demanded. In order to strengthen the isolation in a specific band, elliptic or quasi-elliptic filters are needed. These structures are able to provide steep out-of-band rejection with a minimum number of resonators, minimizing the signal interference in adjacent channels and reducing the volume and mass of the component. Flexibility to define the number and prescribe the location of the transmission zeros (TZs) are important features for this kind of filters. They often determine whether a certain filter implementation is suitable for a particular application.

Several techniques can be used to implement filters with transmission zeros [1]. A method that allows great control over the location of the TZs is the extracted-pole technique [2]. With this technique, the transmission zeros are realized using bandstop elements. Combined with the use of non-resonating nodes [3]–[5], this design methodology becomes highly modular, although it still involves an important amount of optimization to obtain the structure physical dimensions.

For waveguide components, it is common to find solutions that implement cross-couplings between resonators [6]. Multiple paths are created, and the relative phase shift of the signal traveling through all of them produces a cancellation

(destructive interference) at certain frequencies [7]. By properly adjusting the coupling elements in the different signal paths, the designer is able to control the location of the TZs in the complex plane. To improve selectivity of the response, the TZs are placed in the frequency axis. The frequency range (above and/or below the passband) where these TZs can be found is dependent upon the nature (electric or magnetic) of the different couplings involved in the structure. Certain coupling combinations are only able to place TZs below or above the passband. Others are flexible enough to allow the location of TZs both in the upper and lower stopbands. In most applications, simple coupling schemes, such as singlets [8], cascaded triplets and quadruplets [9], are the preferred solution. They are amenable to a modular design procedure, tend to be more robust to manufacturing tolerances and are easier to tune after fabrication.

Amongst these modular schemes, the trisection is one of the most popular configurations to implement filters with asymmetric isolation requirements. A trisection is a third-order structure that realizes a single TZ either above or below its passband. Trisections can be cascaded to create higher-order filters with a flexible control over the location of their corresponding TZs. Each TZ in the response can be directly associated with the cross-coupling in a particular trisection [1]. For that reason, the designer must carefully choose the physical structure (iris, window, probe, loop,...) that will implement the required cross-coupling. The frequency range where the TZ can be located will depend entirely on the range of coupling values that the physical cross-coupling structure is able to provide.

In [10], the HFRW topology was presented as a flexible alternative to implement trisections in rectangular waveguide. This topology has the capability of realizing filters with a wide tuning range of the TZs. Also, it allows a very flexible arrangement of the resonators to achieve very compact geometrical topologies. In addition, due to the physical symmetry in width, the proposed structures can be manufactured in clam-shell, thus reducing losses and increasing its robustness to manufacturing deviations. Tuning screws can thus be avoided in many cases, for instance in filters with relative bandwidths greater than 1-2% for Ku-band applications. The use of a clam-shell assembly combined with the absence of tuning screws minimizes the Passive Intermodulation (PIM) introduced by these filters, consequently making them very suitable for satellite applications [1] and experimental set-ups [10], [11]. **However, the work in [10] only explored a particularly simple configuration providing TZs above the passband.**

C. Carceller, P. Soto, V. Boria and M. Guglielmi are with Universitat Politècnica de Valencia, 46022, Valencia, Spain. Email: carcarc2@upvnet.upv.es, pabsopac@dcom.upv.es, vboria@dcom.upv.es, marco.guglielmi@iteam.upv.es

This work was supported by the Spanish Ministerio de Economía y Competitividad under R&D project TEC2013-47037-C5-1-R.

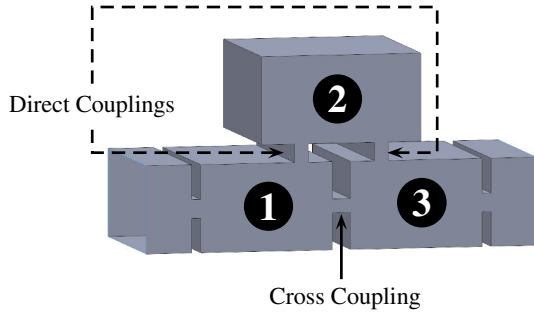


Fig. 1. Basic trisection in the HFRW configuration.

This specific configuration was also used in the channel filters included in [11].

In this paper we extend the previous works by proposing several new configurations for the HFRW topology capable of realizing TZs below the passband. Different alternatives will be provided for the cases where TZs need to be placed either close to the passband or far from it. As it will be shown, due to the nature of the coupling elements within the trisection, some of these configurations are able to provide multiple TZs. Insight into how to control the additional TZs independently of the ones realized by the trisection will also be provided. Likewise, the limitations in the tuning range of these additional TZs will be discussed. To validate our approach, a five-order filter with four TZs will be designed and manufactured. Measured results will be compared with simulations carried out by several available EM software tools.

II. ALTERNATIVE PHYSICAL IMPLEMENTATIONS OF HFRW TRISECTIONS

The design of HFRW filters [12] is based on the interconnection of trisections similar to the one shown in Fig. 1. From a circuit point of view, each of the triplets included in the filter is responsible for the introduction of one TZ and three poles. For the sake of manufacturing simplicity, this type of filters generally make use of centered rectangular apertures in the top or bottom cavity walls to implement direct couplings. Depending on the dimensions and location of these apertures, they provide either electric or magnetic coupling in the frequency band of interest. The in-line physical location of non-adjacent resonators simplifies the implementation of cross-couplings, which can be done in a variety of ways. The particular choice of cross and direct couplings determines whether the TZs are located at finite frequencies above or below the passband. Figure 2 summarizes the specific combination of couplings that provide a TZ on one side of the passband or the other.

The structure presented in [10] included only a particular implementation of HFRW trisections. It contained full-width capacitive slots as direct couplings and a classic inductive window for the cross-coupling. This solution is only able to provide above passband TZs (see Fig. 2). In the present work, however, several new alternatives for implementing both the direct and the cross-couplings are proposed. Although this paper will be focused on the generation of finite TZs below the passband, the physical realization of coupling windows

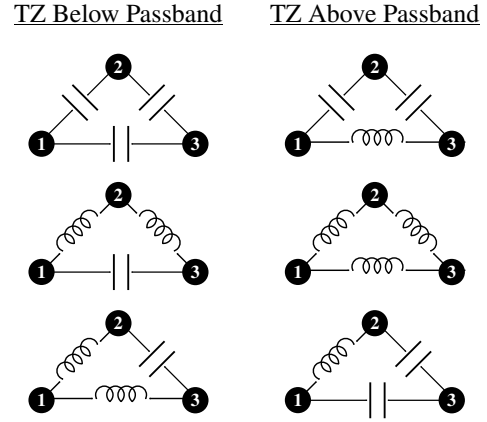


Fig. 2. Coupling combinations in a triplet that provide TZs above or below the passband.

discussed here can also be used to implement triplets with TZs above the passband. With this work, the designer will have a range of coupling elements to choose from. They only need to be properly combined in accordance with the schemes shown in Fig. 2 to implement TZs on either side of the band.

In [13], a similar E-plane triplet implementation in rectangular waveguide was proposed, capable of providing a TZ in either side of the passband. In that work, the direct-coupling apertures connect the front and bottom walls of adjacent resonators, instead of the top and bottom wall connection proposed in the present paper. This results in a different cavity arrangement and a very compact filter layout. The front-bottom connection generates a significantly stronger coupling (compared with the top-bottom one for similar aperture dimensions), prompting the authors in [13] to utilize inductive irises below cutoff to control its level. Even though both structures exhibit very similar features and advantages, the one proposed in this paper provides high flexibility in terms of coupling structures (as described at length in this paper) or generation and control of additional TZ. For instance, the distance from the direct-coupling apertures to the short-circuited end of each resonator can also be easily employed to realize TZs on either side of the band, as demonstrated in [14], [15]. The cross-coupled structures presented in this work can incorporate the aforementioned technique to increase the number of TZs they realize. Nonetheless, the resulting structure may be too large, especially when the TZs have to be located below the passband, thus requiring the use of TE_{102} or higher-order resonators. Even though this is beneficial in terms of losses and manufacturing sensitivity, the resulting increase in filter size and mass may not be acceptable for certain applications (especially for low frequency bands).

This paper is focused on the study of coupling mechanisms in HFRW filters. Several ways to implement triplets with TZs located below the passband are considered in this section. Some of these implementations are suited to place the TZs close to the passband, whereas others are more robust options to implement TZs far from the passband. In addition,

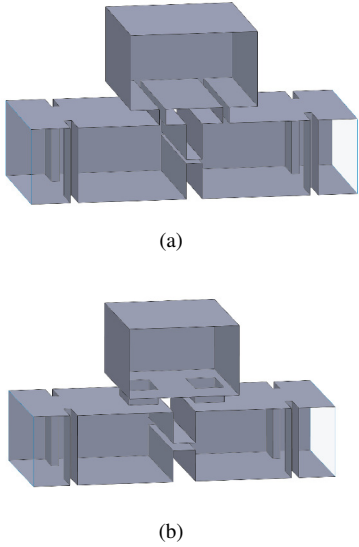


Fig. 3. Two alternatives to implement trisections that provide TZs below the passband using a classical capacitive window as cross-coupling. Side walls have been removed to allow visualization of the interior. a) Capacitive iris used as direct coupling. b) Inductive iris used as direct coupling.

several implementations are capable of providing more TZs than classical triplets. In those cases, simple techniques will be given to adjust these additional TZs and the extent of these adjustments will be discussed.

A. Trisection with classical capacitive cross-coupling iris

The first structure considered, shown in Fig. 3, is a trisection with a capacitive cross-coupling window. For a trisection, the location of the TZ is strongly dependent on the value of the cross-coupling element. As a TZ moves closer to the passband, the cross-coupling value in the triplet increases. Capacitive windows introduce strong couplings, since the passband of the filter is above the cut-off frequency of the window and the fundamental mode at the iris propagates. Therefore, this is an ideal solution to place TZs close to the passband. This type of window guarantees that enough cross-coupling is provided, even if the physical distance between both resonators is large. In contrast, inductive apertures tend to provide lower coupling levels for similar window dimensions, since the iris operates below cut-off in the passband.

To implement the direct couplings, two options have been considered: capacitive irises (Fig. 3a) and inductive irises (Fig. 3b). Generally, the trisection with all capacitive couplings in its core (this is, direct and cross-coupling windows with the same width) is easier to manufacture and design. Given their 2D nature, these geometries are simpler and faster to analyze. However, there are other factors that also influence the decision to implement the direct coupling by irises with a predominantly capacitive or inductive behavior.

The first factor to consider is the position of the TZ. For filters with TZs non-adjacent to the passband, the location of the TZ barely affects the direct coupling level. However, for filters with TZs adjacent to the passband, the location of the TZ has a strong influence on the required direct coupling level. As a TZ moves towards the passband, the direct coupling

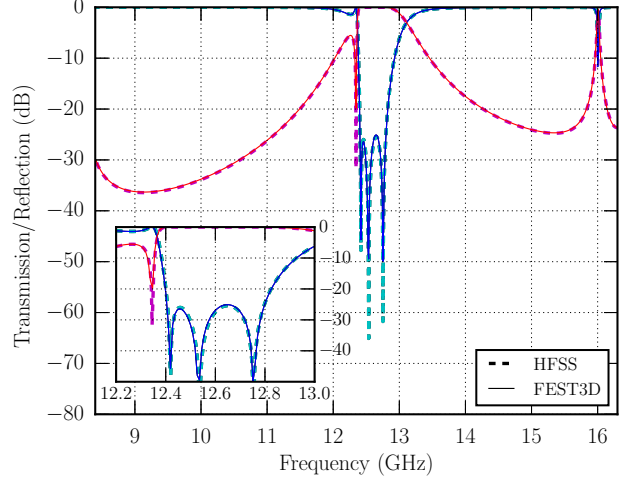


Fig. 4. Comparison between the S-parameter response of the trisection with inductive direct-coupling irises and capacitive cross-coupling window (Fig. 3b), obtained with the modal analysis tool FEST3D [16] and the finite element method solver Ansys HFSS [17]. This triplet introduces a TZ at 12.345 GHz for a filter response centered at 12.6 GHz with a 400 MHz bandwidth. The resonant behavior of the inductive direct-coupling iris generates the undesired resonance at 16 GHz.

level tends to zero. If the required direct coupling level is moderate, the all-capacitive solution in Fig. 3a is preferred, as long as its design and implementation are feasible. However, if the required coupling level is small, the dimension of the capacitive iris implementing the direct coupling may be too small to be physically realizable. In addition, given that the electric field in these irises tends to be high, there is a considerable risk of high-power issues (such as multipactor breakdown) for very small irises.

In those situations where the required direct coupling level is too small, the best option is to use the solution depicted in Fig. 3b. Compared to the all-capacitive solution, the direct couplings in this case are rectangular slots that behave as inductive irises in the passband. These irises are able to yield the same direct-coupling value as the all-capacitive case, but with a much bigger aperture. As a result, the inductive solution avoids the aforementioned mechanical and power-handling issues for filters with TZs extremely close to the passband. Since this is, in nature, a resonant iris, it produces a resonance above the passband. Although it cannot be avoided, its position can be controlled by adjusting the cross-section of the iris. As an example, Fig. 4 shows the response of the triplet depicted in Fig. 3b. This triplet provides a TZ separated from the passband by 55 MHz. The passband is centered at 12.6 GHz with a 400 MHz bandwidth. In the final design, all dimensions are greater than 1 mm, which should guarantee a successful manufacture by milling.

The second factor to consider is the amount of TZs that each option is able to generate in the lower stopband. According to the minimum path rule, a triplet implementing any of the schemes in Fig. 2 should realize one TZ [1]. However, such schemes do not take into account the resonant nature of direct and cross-coupling apertures.

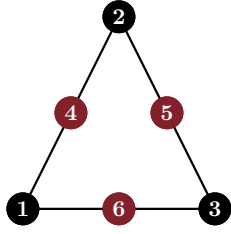


Fig. 5. Sextuplet coupling scheme representing an HFRW trisection. It includes three resonators (4, 5 and 6) that reflect the resonant nature of the direct and cross-coupling windows.

The inclusion of an additional resonating node for each coupling element (modeling its resonance away from the passband) leads to the sextuplet scheme depicted in Fig. 5.

Although the resulting equivalent scheme of a HFRW trisection is not practical for filter design (among other reasons, due to its increased complexity and the limited accuracy of the coupling matrix for wide frequency ranges), it can be useful to provide insight into the structure behavior. In fact, according to the minimum-path rule, this coupling scheme predicts three TZs, in clear contrast with the one corresponding to a conventional triplet (see Fig. 2). The two additional TZs, not accounted for by the triplet, are associated with the direct coupling apertures. The resonance of these elements change the total phase shift of the signal that travels through one of the paths (the one that crosses resonator 2), which leads to a cancellation of the signal at two new frequencies. The specific frequencies where this cancellation occurs are highly dependent on the nature of the direct-couplings, thus not all of the TZs can be prescribed at the lower stopband.

For illustrative purposes, Fig. 6 compares the responses of two sextuplet schemes: one containing capacitive direct-coupling apertures and the other inductive ones. Both coupling matrices have been designed to yield the same passband response and same location of the triplet TZ. When inductive direct-coupling apertures are employed, the additional TZs are located above the passband and outside the spurious-free band (they cannot be simply identified in Fig. 6, since they form a pair of symmetrical zeros around the imaginary axis as a result of the required cross-coupling level). Consequently, only one TZ (associated with the triplet) can be placed in the lower stopband. In contrast, the use of capacitive direct coupling apertures enables the realization of one additional TZ in the lower stopband, as depicted in Fig. 6. Regarding the second additional TZ, it is located below the capacitive resonance (near cut-off), thus its use is not practical.

The results obtained from the EM simulations of the HFRW trisections depicted in Fig. 3 confirms the qualitative conclusions extracted from the enhanced model in Fig. 5, both for the inductive direct-coupling window case (see Fig. 4, with one TZ in the lower stopband) and also for the capacitive direct-coupling case (see Fig. 7, with two TZs in the lower stopband placed above the waveguide cut-off frequency).

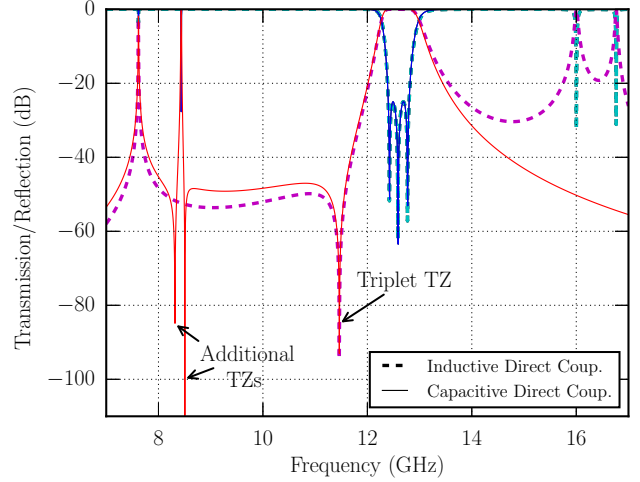


Fig. 6. The sextuplet coupling scheme of Fig. 5 is applied to model the two proposed trisections containing a capacitive cross coupling (Fig. 3). In the capacitive direct-coupling case (solid line), three TZs can be easily identified in the frequency axis. For the inductive direct-coupling structure (dashed line), only one TZ is visible in the lower stopband, whereas the other two TZs form a paraconjugated pair in the complex plane located in the region between the resonances at 16 GHz and 16.8 GHz.

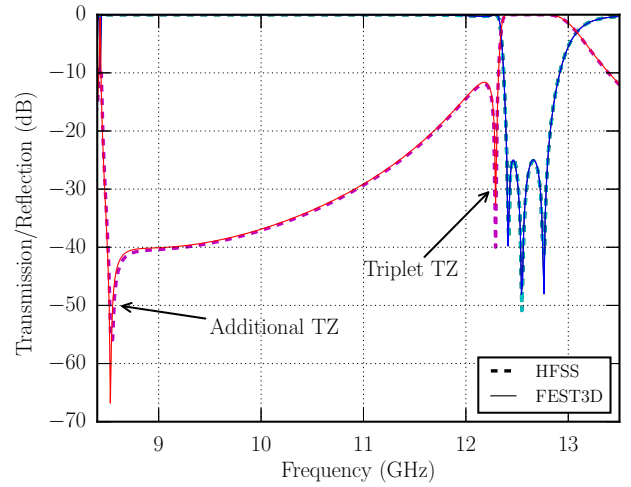


Fig. 7. Comparison between the S-parameter response of the all capacitive trisection (Fig. 3a) obtained with the full-wave modal analysis tool FEST3D and the finite element method solver Ansys HFSS. Two TZs can be easily identified below the passband. The second additional TZ (predicted below the resonances of the capacitive windows) is masked by the cut-off of the waveguide.

B. Triplet with classical inductive cross-coupling iris

In the previous section, it was mentioned that the capacitive cross-coupling window is able to provide high coupling values with relatively small dimensions of the window. This is advantageous when a TZ is to be placed close to the passband, but becomes a burden when the TZ is to be located further away. In those cases, the size of the capacitive coupling may be too small to be manufactured. There are several ways to slightly increase this size. The first one is to increase the length

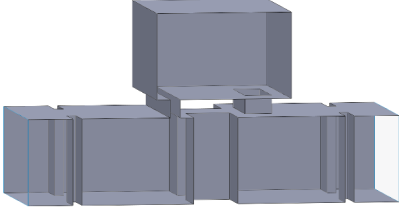


Fig. 8. Trisection with inductive cross-coupling. A capacitive window implements one direct coupling whereas an inductive aperture implements the other direct coupling.

of the cross-coupling window, which comes at the cost of increasing the total length of the filter. In addition, it is obvious that there is a strict geometrical limitation on how much this length can be increased.

Alternatively, the capacitive cross-coupling window can be vertically offsetted towards the central resonator in order to decrease the coupling (effectively allowing an increase in the size of the iris). The increase that can be achieved with this technique is not very large, typically 50% for very small windows.

A more powerful solution is based on the scheme depicted in the bottom-left side of Fig 2. The cross-coupling iris is substituted by a classical inductive window. **Since this window is below cut-off in the band of operation, the coupling it provides, via evanescent modes, is weaker than its capacitive counterpart.** To generate a TZ below the passband, one direct coupling is capacitive while the other one is replaced by a resonant aperture that behaves inductively in the passband. The resulting structure is shown in Fig. 8. This structure is able to provide low cross-coupling levels with moderate dimensions of the inductive cross-coupling iris. Therefore, it is much more robust to manufacturing deviations than its capacitively cross-coupled counterpart for TZs located far from the passband. **As in the all-capacitive case, this particular implementation of a trisection is also able to provide two TZs below the passband, consistent with the sextuplet coupling scheme of Fig. 5.** Figure 9 depicts the response of the trisection shown in Fig. 8, where the two TZs can be identified. **The higher-frequency TZ is the triplet TZ, whereas the lower-frequency TZ is the additional TZ produced by the capacitive direct-coupling aperture. The third TZ (not shown in the plot), is above the resonance of the inductive direct-coupling aperture, thus beyond the spurious-free band. The main inconvenience of this configuration is the presence of the aforementioned resonance in the upper stopband.**

C. Triplet with resonant cross-coupling iris

In order to fulfill specifications that demand TZs far from the passband, but do not allow resonances close to the upper stopband, a third implementation is proposed. This alternative implementation makes use of a resonant cross-coupling structure, where both the inductive and capacitive contributions can be independently adjusted. The idea is to provide additional

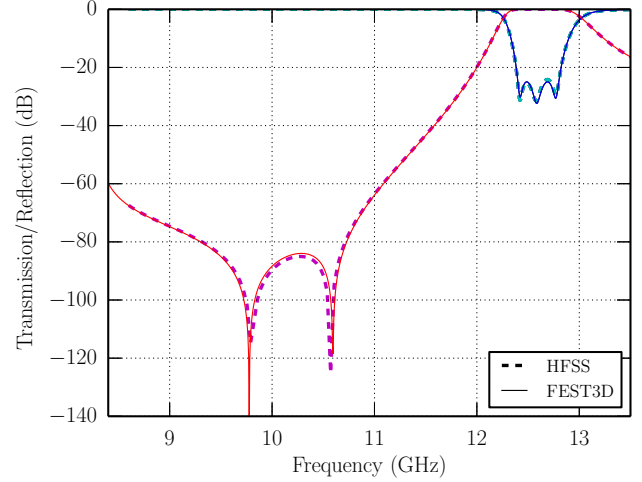


Fig. 9. Response of the trisection with inductive cross-coupling window shown in Fig. 8.

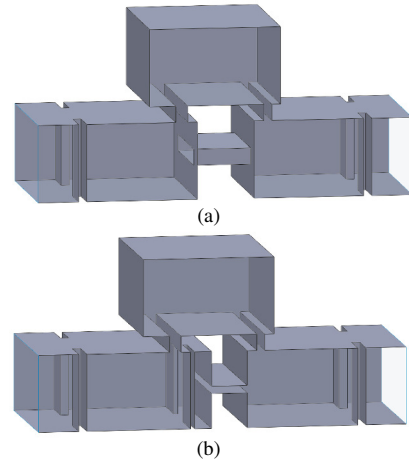


Fig. 10. Trisection with resonant cross-coupling. a) Cross-coupling implemented by a rectangular slot. b) Cross-coupling implemented by the interconnection of an inductive and a capacitive window.

degrees of freedom to generate a specific coupling. In addition to adjusting the iris main dimension (which could compromise the physical realization of the trisection), the specific cross-coupling level can also be controlled by the proper adjustment of the iris resonant frequency. The easiest way to implement such resonant cross-coupling is by means of a rectangular slot, as shown in Fig. 10a. On the one hand, the horizontal dimension of the slot controls the resonant frequency and influences the coupling level. The vertical dimension, on the other hand, mainly affects the cross-coupling level. In practical applications, however, the ability to reduce the horizontal dimension to compensate for an increase in the vertical dimension is limited. Note that the iris must lay above cut-off to behave capacitively. As a result, the vertical size of the cross-coupling cannot be increased significantly (to improve power-handling and feasibility), specially compared to the all-capacitive case described in Section II-A.

A more effective approach involves the resonant cross-

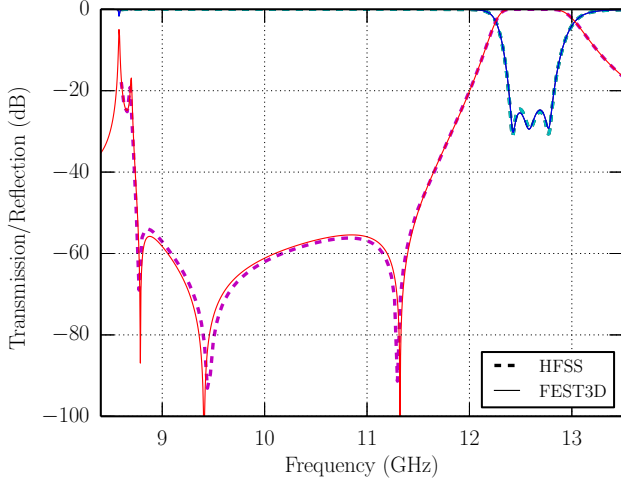


Fig. 11. Response of the trisection with resonant cross-coupling shown in Fig. 10b.

coupling structure shown in Fig. 10b. It is composed of a classical inductive window connected to a capacitive window by a rectangular waveguide. The limiting case where both windows are adjacent to each other is equivalent to the case of Fig. 10a. However, as both irises are physically placed further apart from each other, their mutual interaction becomes weaker, which allows to considerably increase the size of the capacitive iris by decreasing moderately the size of the inductive window. This is a realistic alternative to the topology proposed in Section II-A to locate TZs far from the passband.

Another advantage of this configuration is that, when used in combination with capacitive direct-coupling irises (as the structures shown in Fig. 10), the trisection is able to provide up to three TZs. **This is, once again, compatible with the coupling scheme of Fig. 5 where the resonant frequency of node 6 can be tuned.** By properly adjusting such resonance, the phase shift between the cross-coupled path and the direct-coupled path is altered, and the third TZ can be located in the lower stopband. Figure 11 depicts the response of the structure in Fig. 10b, which generates three TZs. The higher-frequency TZ corresponds with the triplet TZ, whereas the other two are the additional TZs. The simplest way to control the location of the lowest-frequency TZ is to shift the resonance of the iris without altering the cross-coupling level. Also, the distance between the two windows that form the cross-coupling can be used to make slight adjustments to the location of this third TZ.

III. DESIGN PROCEDURE

As previously discussed, the modified coupling scheme of Fig. 5 is an interesting model to understand the behavior of HFRW trisections in the lower stopband. It can be employed to predict the presence of additional TZs in this band, but its application to the complete design of an HFRW filter is limited. The coupling matrix model does not take into account the dispersion of the waveguide elements, and is only a fundamental mode representation

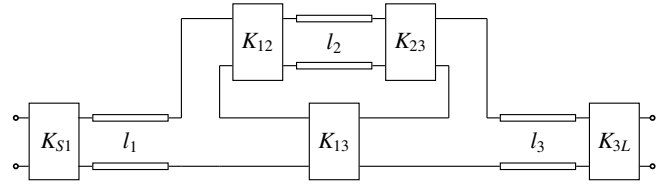


Fig. 12. Distributed equivalent circuit representation of a trisection.

of the structure. Therefore, it does not provide accurate predictions for the position of the additional TZ far from the passband. As a result, it is simpler to perform an initial design of the filter trisections by making use of the classical triplet coupling scheme (considering only the corresponding triplet TZs). Then, a simple methodology can be applied to adjust the location of the additional TZs to prescribed locations.

A. Initial design

From the triplet coupling matrix, the distributed circuit shown in Fig. 12 can be constructed. It contains half-wavelength dispersive transmission lines and inverters. This model takes into account the specific dispersion introduced by the rectangular waveguides implementing the resonators. As shown in [14], the initial values for elements in the distributed model can be extracted from the synthesized coupling matrix as:

$$\begin{aligned} K_{S1} &= M_{S1} \sqrt{\frac{\pi}{2} \mathcal{W}_{\lambda 1}} & K_{3L} &= M_{3L} \sqrt{\frac{\pi}{2} \mathcal{W}_{\lambda 3}} \\ K_{12} &= M_{12} \frac{\pi}{2} \sqrt{\mathcal{W}_{\lambda 1} \mathcal{W}_{\lambda 2}} & K_{13} &= M_{13} \frac{\pi}{2} \sqrt{\mathcal{W}_{\lambda 1} \mathcal{W}_{\lambda 3}} \\ K_{23} &= M_{23} \frac{\pi}{2} \sqrt{\mathcal{W}_{\lambda 2} \mathcal{W}_{\lambda 3}} \end{aligned} \quad (1)$$

where M_{ij} are the non-diagonal elements of the coupling matrix, and $\mathcal{W}_{\lambda i}$ is the wavelength fractional bandwidth of resonator i . The diagonal components of the coupling matrix M_{ii} represent frequency-independent susceptances in the low-pass domain. Once these susceptances are transformed into the bandpass domain, the resonant frequency for each resonator in the filter can be determined according to the formula:

$$f_{ri} = \frac{1}{2} \left[-M_{ii}W + \sqrt{M_{ii}^2 W^2 + 4f_0^2} \right] \quad (2)$$

where f_0 and W are the filter center frequency and bandwidth, respectively. From these resonant frequencies, the line lengths l_i are directly obtained.

From the distributed model, the physical dimensions of the filter can be extracted by using a classical EM-based procedure [18]. Some dimensions in the filter must be set beforehand: the vertical distance between adjacent resonators l_d and the length of the stubs l_s (see Fig. 13a). In order to maintain a compact structure with TE₁₀₁ cavities, the stub lengths have been set to a small value. This particular choice avoids the generation of extra TZs in the response (see [14], [15]), but allows us to focus on the effects under study on this paper. Next, we can proceed with the structure extraction. The first elements to

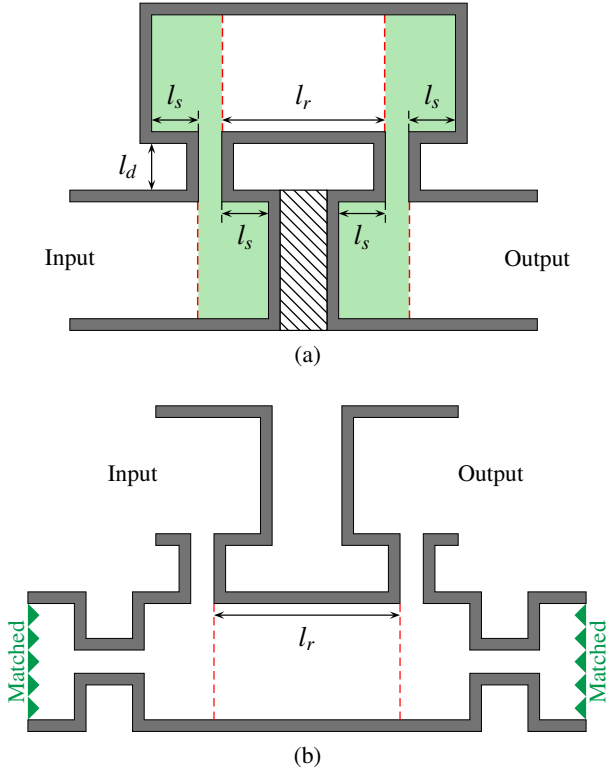


Fig. 13. E-plane cut of a trisection. a) Topology employed to tune the resonance of the central cavity. The hatched area below this cavity indicates the space that can be used to implement the cross-coupling. In advance of the resonance tuning, the shaded area has been adjusted until it has the same behavior as the corresponding direct coupling impedance inverter at the filter center frequency. b) Topology employed to tune the resonance of a cavity with two cross-coupling irises and two direct-coupling irises.

extract are the input/output and direct couplings. In both cases, the dimension of the window that implements each coupling is adjusted until it behaves like the corresponding impedance inverter at the filter center frequency. For the direct couplings, the shaded section of Fig. 13a is used to compare its behavior with the inverter.

Having determined the dimensions of the direct couplings, the next step is to adjust the resonance of the cavities with cross-couplings above or below them. The reason is that, once the dimension of these cavities is determined, the space left to implement the cross-coupling above or below them will be known. This is illustrated in Fig. 13a, where the hatched area represents the space left to implement the cross-coupling after determination of l_r . To adjust the resonance, the distance l_r is shifted until the peak of the reflection coefficient is centered at the appropriate frequency defined by (2).

After the adjustment of l_r , the length of the cross-coupling window below such resonator is known. Then, the iris shape is adjusted to provide the same response as the corresponding impedance inverter at the filter center frequency. Once all the cross-coupling windows are found, the remaining cavities can be adjusted. The structure employed to adjust the length of cavities having cross-coupling windows attached to them is shown in Fig. 13b. All irises are attached to the cavity, to compensate for their loading effect. To avoid reflections, cross-

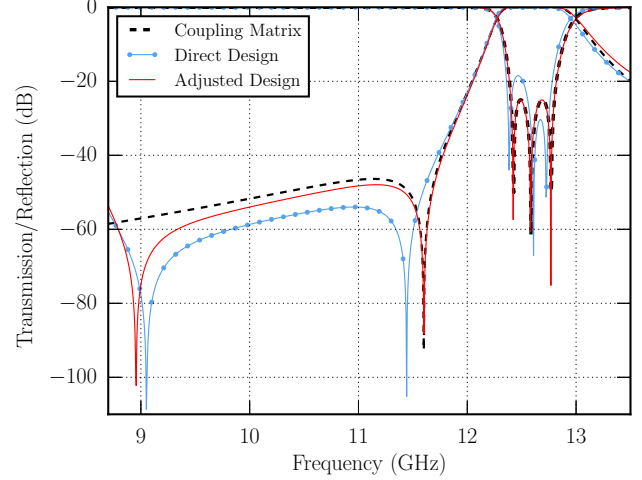


Fig. 14. Response of the example trisection after application of the initial design procedure. The triplet is centered at 12.6 GHz with 400 MHz bandwidth. The coupling matrix response (for a triplet coupling scheme) is compared with the response obtained after direct application of the design procedure and, also, the final response after optimization.

couplings are matched at their output ports.

A response very close to the desired one is obtained after the application of this simple and systematic design procedure. Then, a final adjustment of the dimensions of the filter is performed to compensate for the mutual interactions not previously considered. Finally, a response highly coincident with the one predicted by the coupling matrix is obtained.

As an example, this initial design procedure is applied to a simple all-capacitive triplet in WR-75 waveguide centered at 12.6 GHz with 400 MHz bandwidth and two TZs at 10.5 GHz and 11.6 GHz. The synthesized coupling matrix, considering only the TZ at 11.6 GHz, is:

$$M = \begin{bmatrix} -0.0791 & -1.1951 & -0.2879 \\ -1.1951 & 0.2550 & -1.1951 \\ -0.2879 & -1.1951 & -0.0791 \end{bmatrix} \quad (3)$$

with $R_s = R_L = 1.4918$. By using (1) and (2), the inverter values and resonant frequencies are:

$$\begin{aligned} K_{S1} = K_{3L} &= 0.3492 & K_{13} &= -0.0235 \\ K_{12} = K_{23} &= -0.09769 & & \\ f_{r1} = f_{r3} &= 12.616 \text{ GHz} & f_{r2} &= 12.549 \text{ GHz}. \end{aligned} \quad (4)$$

Following the design procedure to transform the circuit model into a physical structure, the obtained response is similar to the one provided by the coupling matrix. This response can be seen in Fig. 14 with the label “Direct Design”. Afterwards, the dimensions are slightly adjusted to fulfill the passband specifications. This response (labeled “Adjusted Design” in Fig. 14) is equivalent to the one provided by the coupling matrix from the passband to the first TZ. Unfortunately, the location of the second TZ, at 8.9 GHz, is far from the prescribed frequency of 10.5 GHz. In the following subsection, a procedure is proposed to adjust the location of this additional TZ.

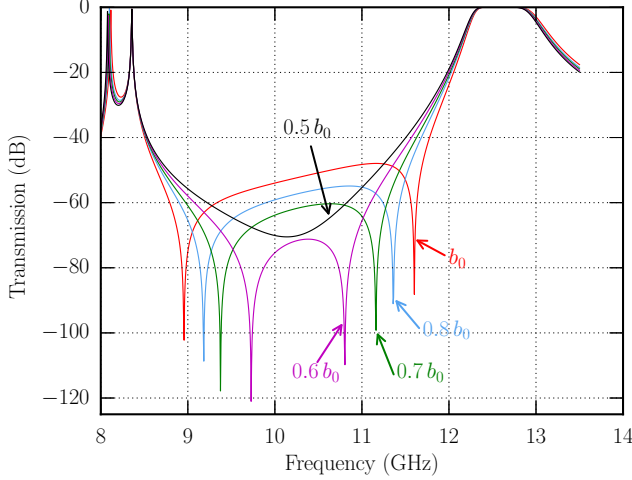


Fig. 15. Using as reference the adjusted design depicted in Fig. 14, the height b_0 of the capacitive cross-coupling window is reduced. As this parameter decreases, the TZ introduced by the triplet moves towards lower frequencies, whereas the additional TZ moves towards higher frequencies.

B. Control over the location of the additional TZ

The exact location of the additional TZ is not simple to determine before the physical structure is obtained. It is highly dependent on the specific phase shifts introduced by the direct- and cross-couplings. Given an initial physical structure, this section proposes a procedure to tune the location of this TZ.

To adjust the location of the additional TZ, the phase shift of one signal path must change with respect to the other path. The more direct way to do so is by modifying the cross-coupling window. This changes the location of the additional TZ but, unfortunately, it also alters the location of the TZ corresponding to the triplet. When the cross-coupling is reduced, the additional TZ moves towards higher frequencies whereas the triplet TZ moves towards lower frequencies, effectively approaching each other. As with any pair of TZs, when they coincide at the same finite frequency (providing a double TZ), their mutual interaction moves them away from the imaginary axis ($s = j\omega$) to paraconjugated complex frequencies. This effect is shown in Fig. 15. Taking as an example the triplet whose response is depicted in Fig. 14, the height of the capacitive cross-coupling is changed between the original size b_0 and half this size (the other dimensions are kept unaltered). As it can be seen, both TZs approach each other until they are no longer visible in the S-parameter response.

Since this technique is not adequate to control the location of the additional TZ independently of the location of the TZ introduced by the triplet, an alternative is proposed. It focuses on adjusting the length of the path that crosses the middle resonator. In order to do so, the length of the direct coupling windows can be increased or decreased (length l_d in Fig. 13). Unfortunately, a change in the length of such window also affects, to some extent, the direct coupling level. As l_d decreases, the direct coupling level slightly increases, thus introducing a small shift on the triplet TZ towards lower frequencies. At the same time, the additional TZ moves

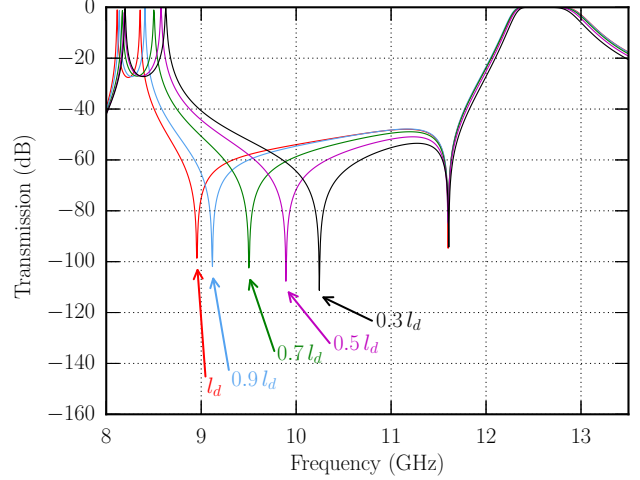


Fig. 16. Starting from the design example shown in Fig. 14, the length l_d that separates vertically the adjacent cavities is reduced. As this length decreases, the additional TZ moves towards higher frequencies (after adjustment of the couplings).

definitely towards higher frequencies. In this situation, the designer can readjust the direct-coupling window to recover the original coupling level. It will be immediately apparent how the additional TZ is now located at a higher frequency than initially, since the total phase shift has decreased. In some instances where there is a strong interaction between direct and cross-coupling windows, it may also be necessary to slightly adjust the cross-coupling window to place the triplet TZ exactly at the original frequency.

The resulting effect after application of this procedure is depicted in Fig. 16. Starting from the designed triplet (see Fig. 14) the length of the two direct-coupling windows l_d is reduced. Then the coupling windows are adjusted to recover the original location of the triplet TZ. As can be seen, the additional TZ effectively moves towards higher frequencies. **Another consequence is that the spurious-free range is reduced. When the triplet TZ is not adjacent to the passband, this effect is limited, as shown in Fig. 16: the additional TZ can be shifted within a large frequency range while the spurious-free range is not considerably reduced. However, when the triplet TZ is very close to the passband, a shift of the additional TZ towards higher frequencies is accompanied by an equivalent reduction in the spurious-free band.**

For trisections with capacitive direct couplings, the change in length can be easily computed. If the additional TZ must be shifted between the original frequency f_{TZ} and the objective frequency f_{obj} , the total length increase can be computed as:

$$\Delta l = \frac{\pi}{\beta(f_{TZ})} - \frac{\pi}{\beta(f_{obj})} \quad (5)$$

where $\beta(f)$ is the phase constant for the fundamental mode in the direct-coupling iris at frequency f . Since the length of both couplings must be equal, the increment Δl must be equally split between the two irises. In the case of triplets with one inductive and one capacitive direct-coupling window, this

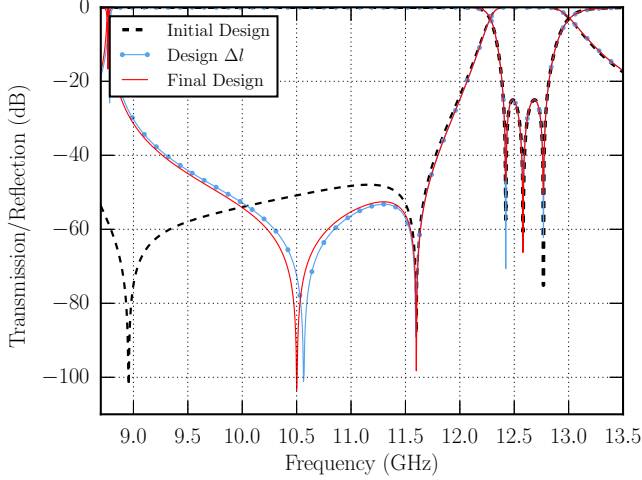


Fig. 17. Final adjustments to the design example in order to move the additional TZ from 8.9 GHz to 10.5 GHz.

equation can be just used as a starting reference to adjust the length of the capacitive one. Additional fine tuning is required in those cases.

This simple method is applied to the designed filter of Section III-A to adjust the location of the TZ from 8.9 GHz to 10.5 GHz. Equation (5) is used to estimate the length decrease of the direct coupling. The resonances and coupling windows are adjusted to recover the passband response and also the original location of the triplet TZ. The response obtained after this procedure is shown in Fig. 17 (labeled "Design Δl "). The additional TZ is not located exactly at 10.5 GHz but very close to this value, at 10.57 GHz. In order to place it at exactly 10.5 GHz, the triplet is re-optimized, adjusting also the length l_d . The final response, having both TZs located at their prescribed frequencies, can be also seen in Fig. 17, labeled as "Final Design".

IV. EXPERIMENTAL RESULTS

This last section considers the design of a five-pole tuning-less filter centered at 12.6 GHz with a bandwidth of 400 MHz and 25 dB return loss. Filter ports and cavities are implemented in standard WR75 waveguides. The in-band specifications are the same as the upper-band Tx filter presented in [10]. In contrast, the filter presented here must introduce 35 dB of attenuation in an adjacent channel separated 130 MHz from the lower passband edge, and at least 100 dB between 8.7 and 11 GHz. These electrical specifications force the introduction of TZs both close to the passband and far from it. They can be satisfied by the cascade connection of two trisections providing 2 TZs each. To deal with the attenuation on the adjacent channel, an all-capacitive trisection is used. The cross-coupling window has been offsetted to guarantee a height greater than 500 microns for manufacturing reasons. In addition, the extra TZ provided by this triplet (at 8.65 GHz) can be used as an aid in providing the out-of-band rejection. Cascaded with this first triplet is a second one that makes use of the configuration presented in Section II-B. The objective of this triplet, which

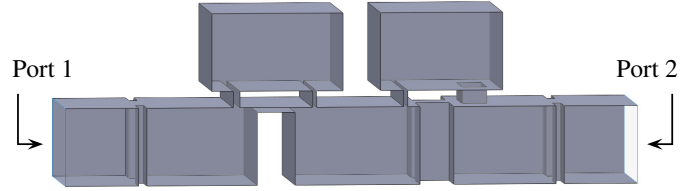


Fig. 18. Geometry of the designed five-pole filter. Two trisections are cascaded: one with all-capacitive couplings and the other with two inductive and one capacitive coupling.

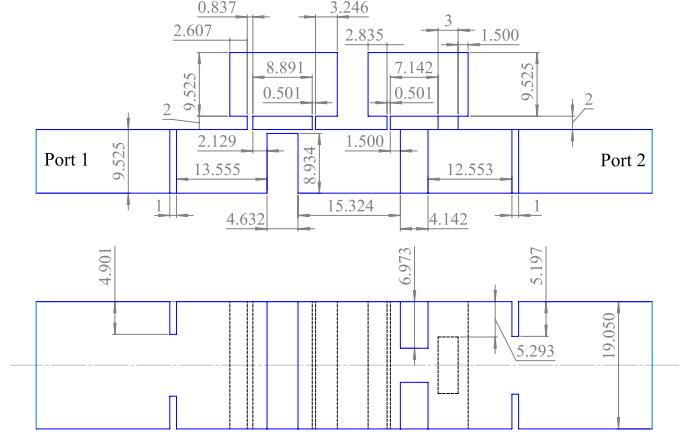


Fig. 19. Side and bottom view of the designed filter along with all dimensions (in mm).

provides TZs at 9.8 GHz and 11 GHz, is to create the rejection band away from the passband. This configuration has been preferred to the one employing a resonant cross-coupling due of its simplicity and robustness. **In addition there are no requirements associated with the upper stopband, which could be potentially affected by the resonance of the inductive coupling window.** The physical structure of the designed filter can be seen in Fig. 18.

Even though a coupling matrix representing a triplet is not able to predict the position of all the TZs, it is a good starting point to determine initial values for the cross and direct-couplings, as well as the resonant frequency of the different resonators. In order to generate this coupling matrix, only the two TZs with higher frequency are considered.

Once an initial dimensional synthesis of the filter is performed, the additional TZs can be adjusted as explained in Section III-B. Optimization of the overall structure is also required. Thanks to the high degree of symmetry of this structure, it can be analyzed rigorously and efficiently with modal methods, which, in turn, allow to speed up the design and optimization process. The commercial software FEST3D, based on these modal methods, has been used to perform the design and optimization. The final optimized dimensions of the prototype can be seen in Fig. 19.

A prototype of this filter has been fabricated in aluminum using a tuning-less clam-shell assembly (see Fig. 20). **The prototype has been manufactured by CNC machining, except for the narrow capacitive windows and the small radius rounded corners, which required spark erosion.** The measured response of this prototype, without any sort of

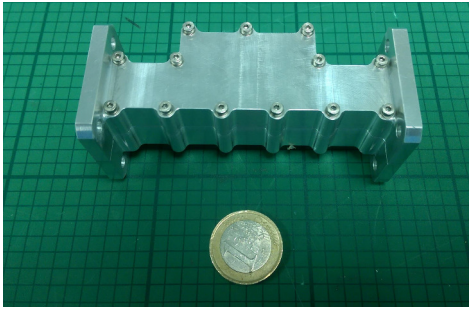


Fig. 20. Photograph of the designed five-pole filter with four TZs.

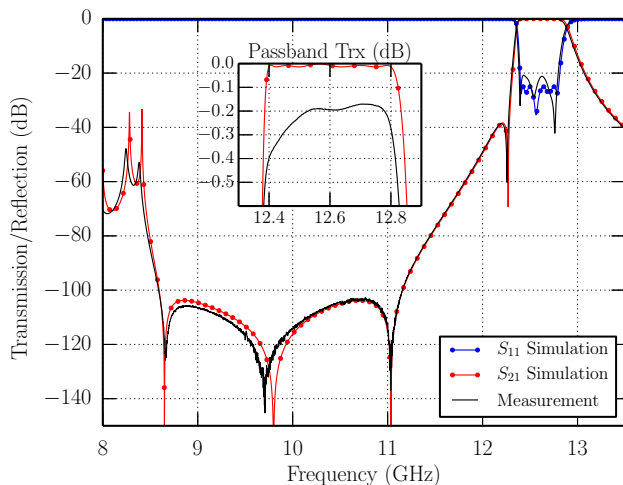


Fig. 21. Response of the designed five-pole filter with four TZs.

tuning, is successfully compared, in Fig. 21, with simulations provided by FEST3D. The measured return losses are better than 20.8 dB in the passband, and the insertion losses better than 0.4 dB. A reduced frequency shift, smaller than 10 MHz, exists between the simulated and measured responses in the passband and in three of the four TZs. The remaining TZ, located at 9.8 GHz in the original design, has just moved 90 MHz in the manufactured prototype. **Finally, it is also worth pointing out that the inductive iris is expected to introduce an unwanted resonance at about 15.6 GHz, beyond the recommended operation range of the filter waveguides.**

V. CONCLUSIONS

The design of HFRW filters with TZs below the passband has been considered in this work. Several novel implementations of these filters have been proposed, and their capabilities, advantages and potential limitations have also been deeply discussed. All the resulting geometries are compact, easy to manufacture and simulate, and suitable for low-loss and low-PIM realizations due to its symmetry in width. Additionally, a simple procedure to design these filters, aided by hybrid EM-circuit models, has been presented. Consequently, from this work a designer can choose the most suitable implementation, and carry out its design in a simple manner.

To sum up, implementations that make use of capacitive cross-coupling irises are adequate to realize filters with TZs close to the passband. Depending on the type of iris used to implement the direct coupling, these structures are able to provide one or two **usable** TZs. There is a certain degree of control for the additional TZ (not predicted by the triplet coupling matrix) by adjusting the length of the direct couplings. For applications that require TZs located far from the passband it is recommended to use filters with inductive cross-couplings, which also are able to introduce two TZs in the lower stopband. However, they generate a resonance in the upper stopband that, in some applications, may be unacceptable. As an alternative, a resonant cross-coupling structure can be used. It has been shown how this solution may introduce up to three TZs per triplet **in the lower stopband**. However, the control of some of the TZs in this structure is limited.

In order to illustrate the capabilities of the proposed implementations, a five order filter composed by two trisections and providing four TZs has been designed and manufactured. Measured results fully validates the practical viability of this new family of filters.

ACKNOWLEDGMENT

The authors are indebted with Mr. Davide Smacchia, from ESA-VSC high-power RF space laboratory, for his assistance with the manufactured prototype.

REFERENCES

- [1] R. J. Cameron, C. M. Kudsia, and R. R. Mansour, *Microwave Filters for Communication Systems: Fundamentals, Design and Applications*. New Jersey: John Wiley & Sons, 2007.
- [2] J. Rhodes and R. Cameron, "General extracted pole synthesis technique with applications to low-loss TE₀₁₁ mode filters," *IEEE Trans. Microw. Theory Techn.*, vol. 28, no. 9, pp. 1018–1028, Sept. 1980.
- [3] S. Amari and G. Macchiarella, "Synthesis of inline filters with arbitrarily placed attenuation poles by using nonresonating nodes," *IEEE Trans. Microw. Theory Techn.*, vol. 53, no. 10, pp. 3075–3081, Oct. 2005.
- [4] S. Cogollos, R. Cameron, R. Mansour, M. Yu, and V. Boria, "Synthesis and design procedure for high performance waveguide filters based on nonresonating nodes," in *Proc. 2007 IEEE MTT-S Int. Microw. Symp.*, Jun. 2007, pp. 1297–1300.
- [5] O. Glubokov and D. Budimir, "Extraction of generalized coupling coefficients for inline extracted pole filters with nonresonating nodes," *IEEE Trans. Microw. Theory Techn.*, vol. 59, no. 12, pp. 3023–3029, Dec. 2011.
- [6] A. Atia, A. Williams, and R. Newcomb, "Narrow-band multiple-coupled cavity synthesis," *IEEE Trans. Circuits Syst.*, vol. 21, no. 5, pp. 649–655, Sep. 1974.
- [7] J. Thomas, "Cross-coupling in coaxial cavity filters - a tutorial overview," *IEEE Trans. Microw. Theory Techn.*, vol. 51, no. 4, pp. 1368–1376, Apr. 2003.
- [8] S. Amari, U. Rosenberg, and J. Bornemann, "Singlets, cascaded singlets, and the nonresonating node model for advanced modular design of elliptic filters," *IEEE Microw. Wireless Compon. Lett.*, vol. 14, no. 5, pp. 237–239, May 2004.
- [9] R. Levy and P. Petre, "Design of CT and CQ filters using approximation and optimization," *IEEE Trans. Microw. Theory Techn.*, vol. 49, no. 12, pp. 2350–2356, Dec. 2001.
- [10] C. Carceller, P. Soto, V. Boria, M. Guglielmi, and D. Raboso, "New folded configuration of rectangular waveguide filters with asymmetrical transmission zeros," in *Proc. 2014 Eur. Microw. Conf. (EuMC)*, Oct. 2014, pp. 183–186.
- [11] C. Carceller, P. Soto, V. E. Boria, M. Guglielmi, and J. Gil, "Design of compact wideband manifold-coupled multiplexers," *IEEE Trans. Microw. Theory Techn.*, vol. 63, no. 10, pp. 3398–3407, Oct. 2015.

- [12] M. Guglielmi, "Hybrid folded rectangular waveguide filter," ESA Patent WO 2015 058 809 A1, 25 Oct. 2013.
- [13] U. Rosenberg, M. Knipp, and S. Amari, "Compact diplexer design using different E-plane triplets to serve contiguous passbands with high interband selectivity," in *Proc. 2006 Eur. Microw. Conf. (EuMC)*, Sept. 2006, pp. 133–136.
- [14] S. Cogollos, P. Soto, M. Brumos, V. Boria, and M. Guglielmi, "Novel rectangular waveguide structures for advanced filter characteristics," in *Proc. 2014 IEEE MTT-S Int. Microw. Symp.*, Jun. 2014, pp. 1–4.
- [15] P. Soto, V. E. Boria, C. Carceller, S. Cogollos, M. Guglielmi, and D. Smacchia, "Practical design of rectangular waveguide filters with a capacitive building block providing an extra transmission zero," in *Proc. 2015 IEEE MTT-S Int. Microw. Symp.*, May 2015, pp. 1–4.
- [16] FEST3D Full-wave Electromagnetic Simulation Tool v.6.8.6. Aurora Software and Testing, Valencia, Spain, 2015. [Online]. Available: <http://www.fest3d.com>
- [17] HFSS v.15. Ansys Inc., Pittsburgh, PA, 2015. [Online]. Available: <http://www.ansys.com>
- [18] S. Cogollos, M. Brumos, V. Boria, C. Vicente, J. Gil, B. Gimeno, and M. Guglielmi, "A systematic design procedure of classical dual-mode circular waveguide filters using an equivalent distributed model," *IEEE Trans. Microw. Theory Techn.*, vol. 60, no. 4, pp. 1006–1017, Apr. 2012.